Development of gas sensor based on fractal substrate structures

Anyan Jiang, Fengchun Tian, Member, *IEEE*, James Anthony Covington, Member, *IEEE*, Maogang Jiang and Zhiyuan Wu

***Abstract*—Gas sensor plays a key role in many applications with sensitivity being a critical performance characteristic. Increasing the surface area of gas sensing material is one approach that can increase sensitivity. Fractal geometries, which have large specific surface area and special fractal dimension, have previously been successfully used in the design of macro and microstructures of gas sensors to improve their performance. In this paper, the influence of geometrical structure of the substrate on the gas sensor performance has been investigated. Two fractal structures (Koch snowflake and Menger sponge) and one traditional structure (Cylinder) were fabricated by 3D printing and coated in Ag:MWCNTs based sensing materials. The fabricated sensors were tested with nitrogen dioxide at different temperatures and humidity. Experimental results show that the sensitivity of gas sensors with fractal structures is increased more than twice that of those with traditional geometrical structures.**

***Index Terms*—Gas sensor, Fractal geometry, Specific surface area, Sensitivity, 3D printing technology.**

I. Introduction

GAS sensors have been widely used in many fields, including environmental monitoring [1], food safety [2] and medical diagnostics [3]. Commonly used gas sensors are based on semiconducting [4], electrochemical [5] and biosensing principles [6]. However, the sensitivity and/or LoD (Limit of Detection) of many kinds of gas sensors is not sufficient for some applications, requiring more sophisticated analytical techniques to be used [7, 8]. Many different approaches have been investigated to improve the sensor's LoD. Depending on the sensing mechanism, it could include changing the microstructure of gas sensing film (e.g. grain size) [9] or adding dopants or impurities [10]. However, the search for new ways to improve the sensitivity/LoD remains an on-going focus of gas sensor research.

Previously, special structures, such as core/shell nanostructures [11, 12] and hollow nanoflowers [13], have been developed to improve the performance/sensitivity of gas sensors. A more recent approach is to use fractal geometry [28]. A remarkable feature of fractal geometry is its self-similarity, i.e., the local shape/structure of a system is similar to its global shape/structure [14, 15]. This similarity makes the surface area of fractal bodies much greater than that of traditional Euclidean shapes. Therefore, fractal theory provides an opportunity to develop new gas sensor structures, which in turn, could improve sensitivity [16].

Most previous work has focused on creating sensing films with fractal features. For example, V. A. Moshnikov *et al*. [17, 18] enhanced the sensitivity of a metal oxide sensing film by the formation of gas sensing layers with percolation cluster fractal structure near the percolation threshold. N. K. Plugotarenko *et al*. [19] investigated the gas sensing performance of $SiO_2 \cdot SnO_x \cdot CuO_y$ nanofilms with different fractal structures, which indicated that the maximal gas sensitivity is obtained at the transition of one type fractal structure to another. Zelio Fusco *et al*. [20] enhanced the performance of their gas sensors by integrating tailored dielectric fractals of TiO_2 nanoparticles on Au nanodisk surfaces.

Different fractal structures have different effects on sensing films. Films with porous [21, 22] and core/shell [23, 24] fractal structures have a larger fractal dimension and specific surface area, which can result in higher sensitivity. For films with dendrite-like nanocrystals, a smaller fractal dimension corresponds to finer branches and smaller breakdown voltages, which results in a higher sensitivity [25]. For films with relief fractal structures, a lower fractal dimension corresponds to higher crystallinity, which again results in a higher sensitivity [26, 27].

The application of fractal structures to the substrate of a gas sensor is also a potential way to improve its sensitivity. Traditional gas sensor substrates are mainly of cylindrical or planar geometries, which do not have large specific surface areas, such as the sensors made by Figaro (Japan). Fig. 1 (a) illustrates the structure of a typical semiconductor gas sensor with micro-heating plate, while Fig. 1 (b) shows a zoom-in photo and illustration of a typical semiconductor gas sensor

This work is supported by the National Natural Science Foundation of China under Grant 62171066. (*Corresponding author: Fengchun Tian, J. A. Covington*)

Anyan Jiang and Zhiyuan Wu are with the School of Microelectronics and Communication Engineering, Chongqing University, 174 Sha Pingba, Chongqing, P.R. China (e-mail: 20161202003@cqu.edu.cn; wuzhiyuan@cqu.edu.cn).

Fengchun Tian is with the Chongqing Key Laboratory of Bio-perception & Intelligent Information Processing and the School of Microelectronics and Communication Engineering, Chongqing University, 174 Sha Pingba, Chongqing, P.R. China (e-mail: FengchunTian@cqu.edu.cn).

James Anthony Covington is with the School of Engineering, University of Warwick, Coventry, CV47AL, UK (e-mail: J.A.Covington@warwick.ac.uk).

Maogang Jiang is with the Department of Electrical and Electronic Engineering, Chongqing University of Technology, 69 Banan, Chongqing, P.R. China (e-mail: jmg1993@163.com)

with a cylindrical substrate.

For planar sensors, the authors have previously used electrodes formed from fractal structures to enhance gas sensor performance [28]. In this paper, we report on the design of a new gas sensor substrate based on fractal geometry and compare it with traditional cylindrical geometries. 3D printing was used to fabricate the sensor substrates with different geometries. Ag doped multi-walled carbon nanotubes (Ag:MWCNTs) was synthesized as the sensing material to validate our concept, and nitrogen dioxide was selected as the test gas to verify the effectiveness of our sensor substrates.

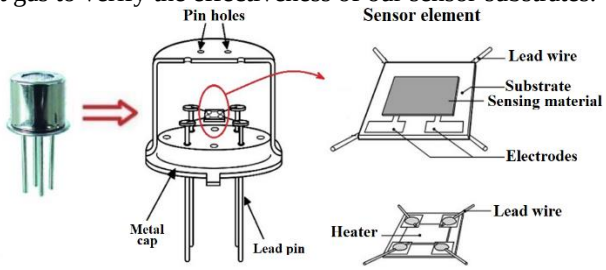

(a)

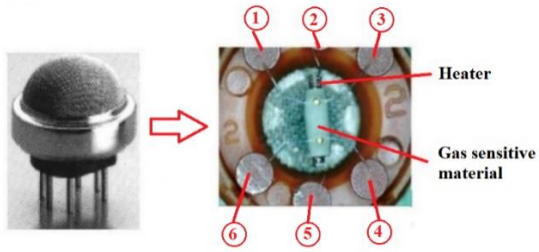

(b)

Fig. 1. Structure of a typical semiconductor gas sensor with micro-heating plate (a) and the zoom-in photo of a typical semiconductor gas sensor with a cylinder structure (Pin 1, 3, 4 and 6 are sensing signal electrodes, pin 2 and 5 are heating electrodes) (b).

II. Fractal Geometry

A. Fractal Structure

There are many geometrical cubes with fractal structures, which have a wide range of characteristics. For example, the Koch snowflake has an infinite perimeter in a limited area, and the Menger sponge is a universal space curve, i.e., any curve is also a homeomorphous subset of itself. Menger sponge is also a bounded, closed set with zero Lebesgue measure, and its Hausdorff dimension is ln20/ln3. Among all the characteristics, the most useful feature of these structures is the large surface area under limited volume (or the large surface area to volume ratio). In most cases, the gas sensing material is coated on the surface of sensor substrate, and so the large surface area to volume will increase the contacting area between the sensing film and the target gas, which could potentially lead to a gas sensor with high sensitivity.

Researchers have studied the area to volume ratio of several fractal geometries [16]. The surface area to volume ratio for Koch snowflake cube, Koch pyramid, Koch tetrahedron, Sierpinski tetrahedron, Menger sponge, and Cylinder in the *k*-th iteration are shown in Fig. 2. It indicates that the fractal geometries have larger structural area than that of traditional Euclidean ones (e.g., cylinder and sphere), and that the Menger sponge has the largest surface area to volume ratio. In addition, the greater the number of iterations, the higher the surface area to volume ratio. The Koch snowflake cube and Menger sponge were used in this work and are shown in Fig. 3 with different iterations.

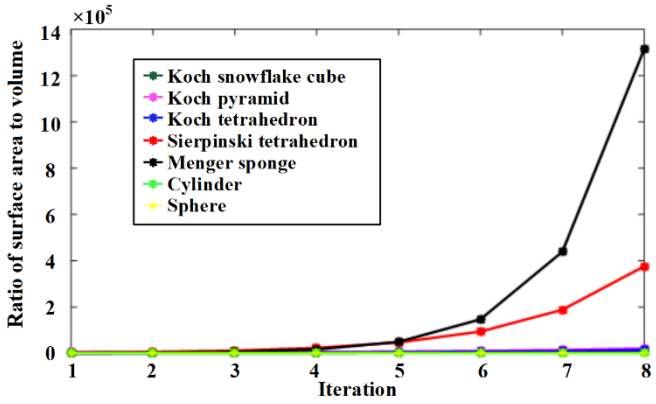

Fig. 2. Ratio of surface area to volume of the seven typical cubes.

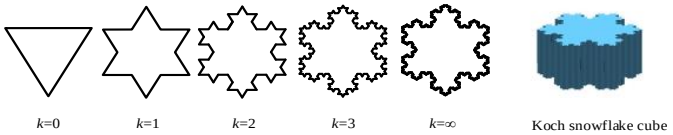

(a)

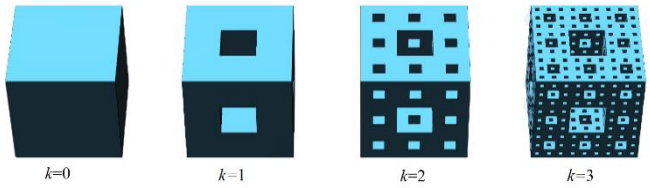

(b)

Fig. 3. Construction processes of Koch snowflake cube (a) and Menger sponge (b) (*k* is the number of iterations).

Assuming the initial side length of Menger sponge and Koch snowflake cube, and the number of iteration of fractal structure are a, a_1 and k, respectively. The surface areas of these fractal structures can be defined as:

$$S_{\text{Menger}}=(2^{2k+1}\times 5^{k}+2^{3k+2})\times\frac{a^2}{3^{2k}}$$

$$S_{\text{Bottom of Kochsnow cube}}=S_{\text{Kochsnow}}=\frac{\sqrt{3}}{4}a_1^{\,2}+\frac{\sqrt{3}}{12}\times\frac{9}{5}\times[1-(\frac{4}{9})^{k}]a_1^{\,2} \quad (1)$$

$$S_{\text{Lateral of Kochsnow cube}}=L_{\text{Perimeter of Kochsnow}}h=3\times 4^{k}\times\frac{a_1 h}{3^{k}}$$

B. Sensor Substrate made by 3D Printing

In our experiment, three kinds of sensor substrates (Koch snowflake cube and Menger sponge, as stated earlier, and a cylinder for reference) were designed. The ‘iteration times’ of Koch snowflake cube and Menger sponge were set as k=4 and k=3, respectively, and the initial side lengths were set as 19.6 mm and 16.2 mm, respectively. The outer radius of Cylinder

was 9.1 mm. The height of these geometries was set at 16.2 mm. The Menger sponge, Koch snowflake cube and Cylinder substrates were designed by 3D modeling software and shown in Fig 4(a). The sensor substrates were fabricated by 3D printing using a nylon filament (P396, EOS, Germany), which has an accuracy/repeatability of 0.1mm. Only those substrates with group deviation less than 5% were chosen. Fig (b) shows a photo of these fabricated substrates.

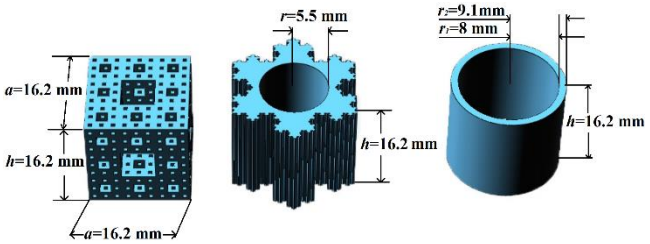

(a)

(b)

Fig. 4. Models of Menger sponge, Koch snowflake cube and Cylinder (a) and a photo of 3D printed substrates.

Generally, the volume is equal to bottom area times height. The volume of Koch snowflake cube, Menger sponge and Cylinder can be calculated as:

$$\begin{aligned} V_{\text{Menger}} &= S_{\text{Bottom of menger}} \times h = a^2 \times h = 4251.528\,mm^3 \\ V_{\text{Koch}} &= S_{\text{Bottom of Kochsnow cube}} \times h = S_{\text{Kochsnow}} \times h \\ &= [\frac{\sqrt{3}}{4} a_1^{\,2} + \frac{\sqrt{3}}{12} \times (1 + \frac{4}{9} + \frac{4^2}{9^2} + \frac{4^3}{9^3}) a_1^{\,2}]h = 4249.471\,mm^3 \\ V_{\text{Cylinder}} &= S_{\text{Bottom of cylinder}} \times h = \pi r_2^2 h = 4251.325\,mm^3 \end{aligned} \tag{2}$$

where a=16.2 mm, a_1=19.6 mm and h=16.2 mm.

The surface area to volume ratio of Menger sponge, Koch snowflake cube and Cylinder are given in Eq. (3), which indicate that the Menger sponge has the largest surface area.

$$\begin{aligned} \frac{S_{\text{Menger}}}{V_{\text{Menger}}} &= \frac{(2^7 \times 5^3 + 2^{11}) \times \frac{a^2}{3^6}}{a^2 \times h} = 1.528\,mm^2 / mm^3 \\ \frac{S_{\text{Koch}}}{V_{\text{Koch}}} &= \frac{2(S_{\text{Kochsnow}} - S_{\text{circular}}) + S_{\text{Lateral area}} + S_{\text{Inner cylindrical surface}}}{S_{\text{Kochsnow}} h} \\ &= \frac{2[\frac{\sqrt{3}}{4} a_1^{\,2} + \frac{\sqrt{3} a_1^{\,2}}{12}(1 + \frac{4}{9} + \frac{4^2}{9^2} + \frac{4^3}{9^3}) - \pi r^2] + \frac{4^4 a_1 h}{3^3} + 2\pi r h}{[\frac{\sqrt{3}}{4} a_1^{\,2} + \frac{\sqrt{3} a_1^{\,2}}{12}(1 + \frac{4}{9} + \frac{4^2}{9^2} + \frac{4^3}{9^3})]h} \\ &= 0.919 mm^2 / mm^3 \\ \frac{S_{\text{Cylinder}}}{V_{\text{Cylinder}}} &= \frac{2S_{\text{Bottom area}} + S_{\text{Outer cylindrical}} + S_{\text{Inside cylindrical}}}{S_{\text{Bottom\_cylinder}} h} \\ &= \frac{2\pi(r_2^{\,2} - r_1^{\,2}) + 2\pi h(r_1 + r_2)}{\pi r_2^{\,2} h} = 0.439\,mm^2 / mm^3 \end{aligned} \tag{3}$$

where r_2=9.1 mm, r_1=8 mm and r=5.5 mm.

III. Experiment

A. Chemicals

Silver nitrate ($AgNO_3$) and Sodium citrate ($C_6H_5Na_3O_7{\cdot}2H_2O$) were purchased from Shanghai Aladdin Biochemical Technology Co., Ltd. All reagents used are of analytic purity and required no further purification. Deionized water was used in all synthesis and fabrication processes. Carbon nanotube dispersion were purchased from Chinese Academy of Sciences Chengdu Organic Chemistry Co., Ltd. and its main characteristics are shown in Table I.

TABLE I
PARAMETERS OF MULTI-WALLED CARBON NANOTUBES

Characteristic	Unit	MWCNTs	Characterization method
Outer Diameter	nm	8-15	HRTEM, Raman
Purity	wt%	>95	TGA & TEM
Length	μm	~50	TEM
Special Surface Area	m^2/g	>140	BET
ASH	wt%	<1.5	TGA

B. Synthesis of Ag:MWCNTs Samples

The classical Lee method was used to prepare the Ag sol [29]. The preparation process of Ag:MWCNTs is shown in Fig 5(a). In detail, 270 mL multi-walled carbon nanotubes (MWCNTs) dispersion with a concentration of 0.5 mg/mL was obtained and ultrasonic dispersed in a beaker for 10 minutes. Then 36 mg $AgNO_3$ and 60 mg $C_6H_5Na_3O_7{\cdot}2H_2O$ were added to the beaker. The as-obtained solutions were magnetically stirred at 95℃ for 45 minutes, and then cooled naturally down to room temperature with continuous magnetic stirring. The resulting products were separated from the reaction medium by centrifuging at 15200 r/min for 1 hour and rinsed with deionized water. The centrifugation process was repeated twice, then 30 mL of deionized water was added for dilution, and ultrasonic dispersion was carried out for 15 minutes.

C. Fabrication and Characterization of gas sensors

Before gas testing, a pair of electrodes and wires were placed on each end of the 3D substrates. The electrodes and wires were then coated and connected by conductive silver paste (LUXIANZI, China). The Ag:MWCNTs solution and the 3D sensor substrates were transferred to a 100 mL Teflon-lined stainless steel autoclave, heated at 95 ℃ for 6 hours. Once the autoclave had cooled down to room temperature, the sensors were rinsed with deionized water and dried in an oven at 60℃ for 30 minutes. The fabrication process is shown in Fig 5(b). The morphological character and microstructure of as-prepared films were characterized by field emission scanning electron microscopy (FESEM, FEI Nova400) with an acceleration voltage of 20 kV, and an energy dispersive X-ray spectroscopy attached to the SEM.

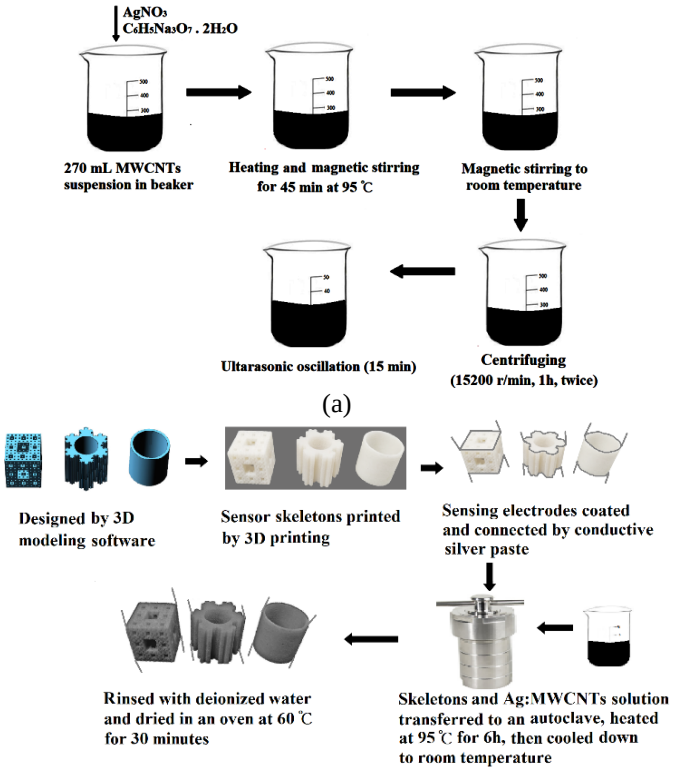

Fig. 5. Preparation of Ag:MWCNTs (a) and fabrication process of sensors (b).

D. Measurement of Sensor Performance

Fig. 6 shows the setup used for sensor testing and the schematic diagram of the test circuit. In total, 15 sensors were used (5 of each type). Inside the test chamber (Teflon coated) a temperature & humidity sensor (SHT15, SENSIRION, Switzerland) was placed. The chamber was put into an electric drying oven (DHG-9053A, SuoKe, China), which was used to control the ambient temperature. A programmable linear DC power supply (SPD3303C, SIGLEVT, China) was used to provide a working voltage for the sensors and the output voltage was measured by a data acquisition card (USB3000, Art Technology, China), with the resultant data transferred and stored on a computer. To avoid oxidation of Ag by O_2, we only used N_2 as the carrier gas, as this study focuses on the sensor substrates. The sensors were first exposed to dry N_2 for 10 minutes, followed by injection of the target gas (NO_2) for a further 10 minutes, then the oven was heated to 70 ℃ for 10 minutes to accelerate the sensor desorption and then cooled down to the experimental temperature, till the sensor returned to its baseline resistance. In these experiments, NO_2 was used at five different concentrations (0.25, 3, 6, 9, 12 ppm). The sensor response to NO_2 was defined here as $S=(R_a-R_g)/R_a$, where R_a and R_g is the resistance of the sensing layer measured in N_2 and NO_2, respectively. Sensitivity is defined as the slope of the linear fitting equation of the response curve.

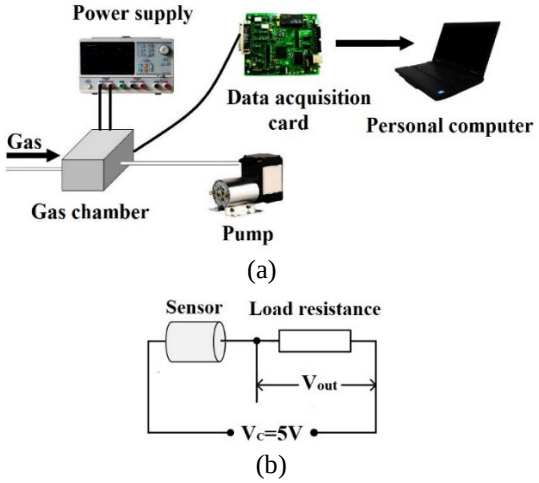

Fig. 6. Setup of the sensor testing (a) and circuit (b).

IV. Results and Discussion

The SEM and elemental mapping images of the Ag:MWCNTs film are shown in Fig 7. Fig 7(a) shows that the arrangement of MWCNTs is disordered and intertwined. The Ag nanoparticles, which are of spherical shape, are effectively modified on the outer wall of MWCNTs. Fig 7(b) shows that many Ag nanoparticles are adsorbed on the surface of MWCNTs. Although there are aggregations of Ag nanoparticles in some places, the overall distribution is relatively uniform. Fig. 8 shows the dynamic response of one of the Menger sponge upon exposure to NO_2 (0.25, 3, 6, 9 and 12 ppm) at 25 ℃ & 10% RH, which exhibits a NO_2 concentration dependent response. The sensor resistance gradually returns to its initial level, after the gas was removed. To speed up this process a heating cycle was also performed before the sensors were returned to the experimental temperature [30].

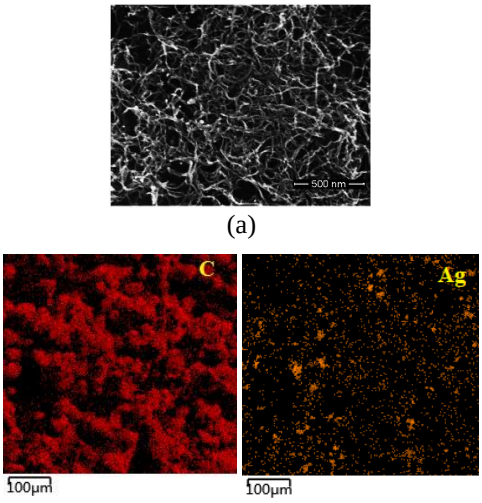

Fig. 7. SEM image (a) and Elemental mapping images (b) of the Ag:MWCNTs film.

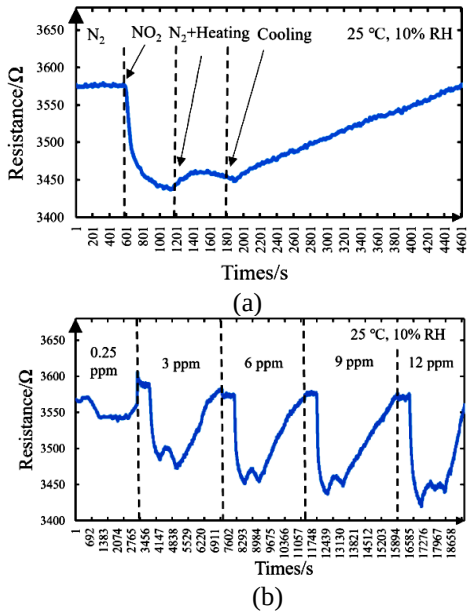

Fig. 8. Dynamic response of a Menger sponge sensor to 9 ppm NO_2 (a) and in different concentration (b) at 25℃, 10% RH.

Fifteen sensors were used (with the three kinds of substrates: Menger sponge, Koch snowflake and Cylinder; Substrate number of each kind is 5) for performance (including repetition) test. Response curves of sensors to NO_2 (0.25, 3, 6, 9 and 12 ppm) at 25 ℃, 10% RH and corresponding piecewise linear fitting equation of different concentrations are shown in Fig 9. This shows that the response of the sensors with Menger sponge and Koch snowflake structures are better than those with Cylinder structures. Here, the sensitivity is proportional to the surface area to volume ratio [16]. Theoretically, the surface area to volume ratio of the Menger sponge, Koch snowflake cube and Cylinder are 1.528, 0.919 and 0.439 respectively. This indicates that the sensors with Menger sponge structures and Koch snowflake structures could potentially have 3.48 times and 2.09 times, respectively, greater sensitivity compared to the Cylinder structure. Fig. 9 (b) shows that sensors with Koch snowflake structures have around 2.18 times the sensitivity compared to the Cylinder structure, at 3~12ppm NO_2. However, the sensors with Menger sponge structures are no better than those with Koch snowflake structures, with an increase in sensitivity of around 2.05 compared to the Cylinder structure. Potential reasons for this, maybe a limitation of the 3D printer, which cannot fully fabricate the internal pore structure. Also, the inner pore structure of the Menger sponge may increase the time taken for the target gas to contact the sensing material, and thus the sensors may not have fully responded by the end of the experimental period. In the future, we will use a micron level printing approaches and update our gas testing system to reduce the time taken for the target gas to arrive at the internal gas sensing surfaces. In addition, this micron level printing may allow us to attain even higher surface area to volume ratios, which theoretically may be 10^5 greater than that of Cylinder (Fig. 2). It can be speculated that much higher sensitivity can be obtained with these substrate structures.

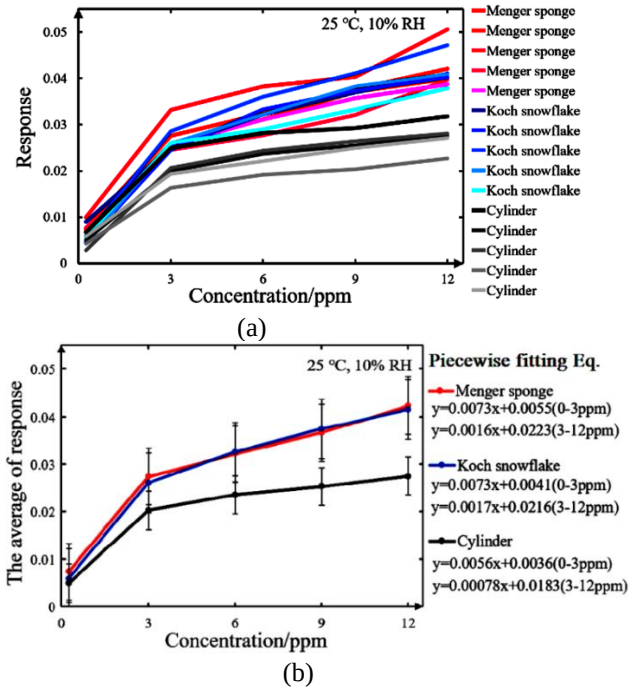

Fig. 9. Response curves (a) and the averaged response curves/fitting Eq. (b) of sensors to NO_2 at 25 ℃, 10% RH.

Gas sensor responses using carbon nanotubes can be affected by temperature and humidity [30]. Thus, experiments were repeated at 40 and 55℃ at 10% RH, with the corresponding results are shown in Fig. 10. The process of gas humidification is described in Fig. S1, Supporting Information. The resistance of the sensors decreased as the temperature increased (Fig. S2, Supporting Information). The responses increased at 40℃ and decreased further at 55℃. This is likely due to the change of adsorption and desorption rate with temperature. There was only one sensor (outlier), with a Cylinder structure that had a higher response than some other sensors with fractal structures (Fig. S3, Supporting Information). Fig. 10 shows that the averaged response of the sensors with Cylinder structure are lower than those with fractal structures.

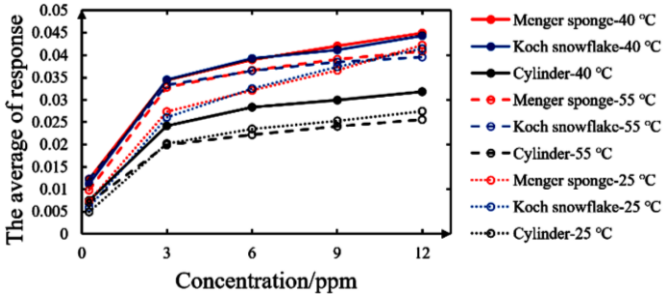

Fig. 10. Averaged response curves of the sensors to NO_2 at 25℃, 40℃ and 55℃ at 10% RH.

The sensing tests of NO_2 (0.25, 3, 6, 9 and 12 ppm) at 30℃, 20% RH, 50% RH and 80% RH were also conducted, and the corresponding results are shown in Fig. 11. The sensor resistance and response increased as the humidity level was raised (Fig. S4, Supporting Information). The reason behind this is associated with the adsorption of water molecules. For MWCNTs, the main absorption route is physical and the

accumulation pores and outer surface of the accumulation, formed by intertwining of MWCNTs, are the main adsorption centers. The adsorption of water molecules weakens the van der Waals force between MWCNTs, which increases the gaps among MWCNTs. This in turn increases the porosity and enhances the adsorption performance. The results indicate that sensors with fractal structures have a higher response than those with a Cylinder structure, except one outlier (Fig. S5, Supporting Information). As can be seen in Fig. 11, the response and sensitivity of sensors with fractal structures are greater than those of Cylinder under different humidity conditions.

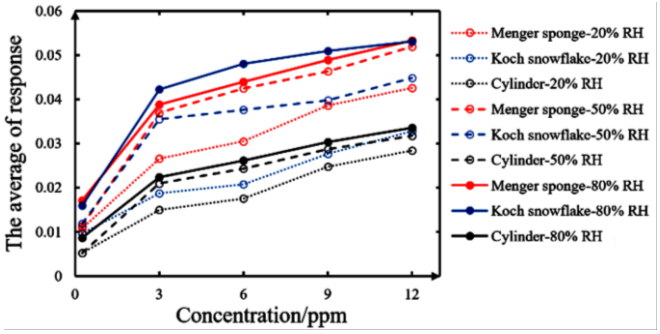

Fig. 11. Averaged response curves of sensors to NO_2 at 20% RH, 50% RH and 80% RH at 30℃.

Fig. 12 shows the stability of one of the Menger sponge sensors at 25℃, 10% RH in N_2 and 300 ppm NO_2. The measurements were conducted for 7 days and the resistances in N_2 and 300 ppm NO_2 were recorded at daily intervals. In Fig. 12, the baseline resistance changes between 3373 Ω and 3377 Ω, while the response resistance varies between 2959 Ω and 2982 Ω. It shows that the maximum deviation of the baseline and response resistances is less than 5% from the initial value, reflecting an excellent stability over the test period (Fig. S6, Supporting Information).

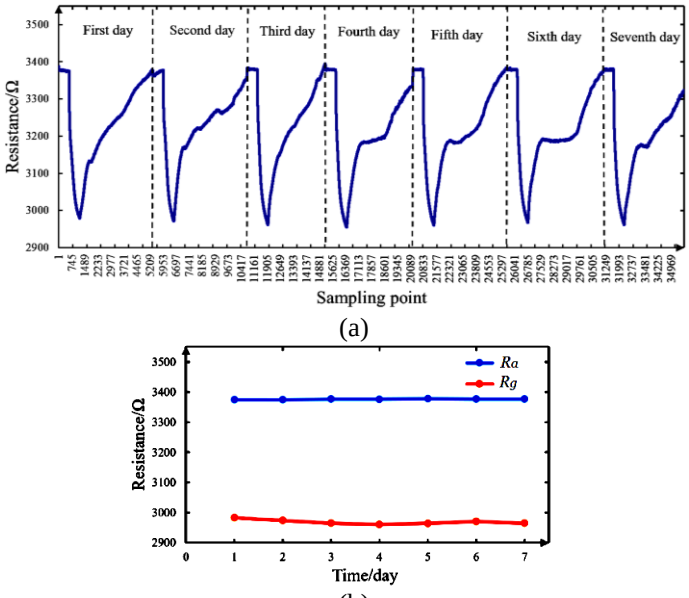

Fig. 12. Week stability tests of sensors to 300 ppm NO_2 at 25°C, 10% RH: the dynamics response curve of one of the Menger sponge sensors to 300 ppm NO_2 (a) and the corresponding baseline resistance R_a and response resistance R_g (b).

This work has shown that using fractal substrate geometries does lead to an increase in response over traditional substrates, at the same scale. A limitation of this study is the dimensions of the substrates generated. However, using micron or even smaller level 3D printing with high accuracy (or similar manufacturing techniques) will produce much smaller substrates and potentially, result in much higher sensitivity and reproducibility. Another limitation of our study is that the structures were fabricated with nylon. It inhibits the use of materials with higher operating temperatures, such as metal-oxides. In our following work, we will investigate the use of 3D printing of ceramic structures to remove this limitation, including the integration of metal heater and electrode structures.

V. Conclusion

In this paper, the influence of substrate structure on gas sensor sensitivity was studied. Fractal theory was applied to the structural design of the gas sensor substrate. Sensors with Menger sponge, Koch snowflake and Cylinder substrate structures were fabricated by 3D printing and NO_2 was used as the target gas to test their performance. Experimental results show that the sensors with fractal structures have a greater response and sensitivity than those sensors with a Cylinder structure. Our next steps will be to develop ceramic based fractal structures allowing much higher operating temperatures or selecting better gas sensing materials, such as metal oxide semiconductor [31] or polymer etc. [32].

Acknowledgment

The authors would like to acknowledge the National Natural Science Foundation of China (62171066) for its fund support.

References

[1] Sun B, Lv H, Liu Z, *et al*., "Co3O4@PEI/Ti3C2Tx MXene nanocomposites for highly sensitive NOx gas sensor with low detection limit," *Journal of Materials Chemistry A*, no.10, Jan. 2021.

[2] A. Loutfi, S. Coradeschi, G.K. Mani, *et al*., "Electronic noses for food quality: A review", *Journal of Food Engineering*, vol. 144, no. 144, pp. 103-111, Jul. 2015.

[3] Zhao, Hongran Liu, Lichao Lin, Xiuzhu Dai *et al*., "Proton-Conductive gas sensor: A New Way to Realize Highly Selective Ammonia Detection for Analysis of exhaled Human breath", *ACS SENSORS*,vol. 5, no. 2, pp. 346-352, Dec. 2020.

[4] Oleksenko L P and Maksymovych N P. "Semiconductor Sensors of Gases Based on Pd/SnO2-Sb2O5 Materials," *Theoretical and Experimental Chemistry*, vol. 57, no. 1, pp. 64-70, May. 2021.

[5] Zhao S, Zang G, Zhang Y, *et al*., "Recent advances of electrochemical sensors for detecting and monitoring ROS/RNS," *Biosensors & Bioelectronics*, vol. 179, pp. 113052, May. 2021.

[6] Ward S J, Layouni R, Arshavsky-Graham S, *et al*., "Signal Processing Techniques to Reduce the Limit of Detection for Thin Film Biosensors," *ACS Sensors*,. vol. 6, pp. 2697-2978, Mar. 2021.

[7] Kruefu V, Wisitsoraat A, Phanichphant S. "Effects of niobium-loading on sulfur dioxide gas-sensing characteristics of hydrothermally prepared tungsten oxide thick film," *Journal of Nanomaterials*, vol. 2015, pp. 1-8, Mar. 2015.

[8] Liu Y, Xu X, Chen Y, *et al*., "An Integrated Micro-chip with Ru/Al2O3/ZnO as Sensing Material for SO2, Detection," *Sensors & Actuators B Chemical*, vol. 262, pp. 26-34, Jun. 2018.

[9] Dey, Ananya. "Semiconductor metal oxide gas sensors: A review", *Materials Science & Engineering, B*, vol. 229, Jan. 2018.
[10] Young, S, J and Z. D. Lin, "Acetone gas sensors composed of carbon nanotubes with adsorbed Au nanoparticles on plastic substrate", *Microsystem Technologies*, vol. 24, no. 10, pp. 3973-3976, Sep. 2018.
[11] Seyed Amirabbas Zakaria, Susan Samadi and Ghasem Asadi Cordshooli, "Synthesis and characterization of zirconium (IV) and vanadium (III) doped CeO2/TiO2 core/shell nanostructures as a gas sensor," *SENSOR ACTUAT A-PHYS*, vol. 318, pp. 112226, Jul. 2021.
[12] Zhao Sikai, Shen, Yanbai, Zhou, Pengfei, *et al.,* "Design of Au@WO3 core−shell structured nanospheres for ppb-level NO2 sensing," *Sens. Actuators B Chem*, vol. 282, pp. 917–926, 2019.
[13] H Gao, Q Yu, K Chen, *et al.*, "Ultrasensitive gas sensor based on hollow tungsten trioxide-nickel oxide (WO3-NiO) nanoflowers for fast and selective xylene detection," *J. Colloid Interface Sci*, vol. 535, pp. 458–468, Feb. 2019.
[14] M Frame et al., Fractal Worlds: Grown, Built, and Imagined[M]. Yale University Press, 2016.
[15] An'an Zhou, Tianning Chen, Xiaopeng Wang, *et al.*, "Fractal contact spot and its application in the contact model of isotropic surfaces," *Journal of Applied Physics*, vol. 118, no. 16, pp. 165307, Oct. 2015.
[16] Tian F, Jiang A, Yang T, *et al.*, "Application of Fractal Geometry in Gas Sensor: A Review," I*EEE Sensors Journal*, vol. 21, pp. 14587-14600, Jul. 2021.
[17] S. S. Nalimova, A. A. Bobkov and V. A. Moshnikov, "Fractal Structure and Electrical Properties of Percolation Sensor Layers," *Smart Nanocomposites*, vol. 7, no. 1, pp. 21-26, 2015.
[18] S. S. Karpova, V. A. Moshnikov, S. V. Mjakin, and E. S. Kolovangina, "Surface functional composition and sensor properties of ZnO, Fe2O3, and ZnFe2O4," *Semiconductors*, vol. 47, no. 3, pp. 369–372, Mar. 2013.
[19] N. K. Plugotarenko, V. V. Petrov, V. A. IvanetzV and A. Smirnov, "Investigation of the formation of fractal structures in SiO2 • SnOx • CuOy thin films prepared by the sol-gel method," *Glass Physics & Chemistry*, vol. 37, no. 6, Sep. 2011.
[20] Fusco Z, Rahmani M, Bo R, *et al.*, "Nanostructured Dielectric Fractals on Resonant Plasmonic Metasurfaces for Selective and Sensitive Optical Sensing of Volatile Compounds," *Adv. Mater*, vol. 30, no. 30, pp. 1800931.1-1800931.11, Jun. 2018.
[21] Khatibani A B and Abbasi M, "Comparison of gas sensing properties of spray pyrolysed VOx thin films," *J MATER SCI-MATER EL*, vol. 26, no. 7, pp. 1-8, Apr. 2015.
[22] Abbasi M, Rozati S M, Irani R, *et al.*, "Synthesis and gas sensing behavior of nanostructured V2O5 thin films prepared by spray pyrolysis," *MAT SCI SEMICON PROC*, vol. 29, pp. 132-138, Jan. 2015.
[23] Sabri Y M, Kandjani A E, Rashid S S A A H, *et al.*, "Candle-Soot Derived Photoactive and Superamphiphobic Fractal Titania Electrode," *CHEM MATER*, vol. 28, no. 21, pp. 7919-7927, Oct. 2016.
[24] Sabri Y M, Kandjani A E, Rashid S S A A H, *et al.*, "Soot template TiO2 fractals as a photoactive gas sensor for acetone detection," *Sens. Actuators B Chem*, vol. 275, pp. 215-222, Aug. 2018.
[25] Chen Z, Pan D, Zhao B, *et al.*, "Insight on fractal assessment strategies for tin dioxide thin films", *Acs Nano*, vol. 4, no. 2, pp. 1202-8, Jan. 2010.
[26] Dimitrov D T, Nikolaev N K, Papazova K I, *et al.*, "Investigation of the electrical and ethanol-vapour sensing properties of the junctions based on ZnO nanostructured thin film doped with copper," *Appl. Surf. Sci*, vol. 392, pp. 95-108, Jun. 2017.
[27] Yakushova N D, Pronin I A, Averin I A, *et al.*, "Investigation of the correlation between gas-sensitive properties and fractal dimension of nanostructured ZnO/ZnO films obtained by the sol-gel method," *IOP Conference*, vol. 387, no. 1, 2018.
[28] Taicong Yang, Fengchun Tian, Anyan Jiang, Covington, *et al.*, "Resistance-capacitance gas sensor based on fractal geometry," *Chemosensors*, vol. 7, pp. 31, Jul. 2019.
[29] Lee P C and Meisel D. "Adsorption and surface-enhanced Raman of dyes on silver and gold sols," *Journal of Physical Chemistry*, vol. 86, no. 17, pp. 3391-339, Apr. 1982.
[30] Han T, Nag A, Mukhopadhyay S C, *et al.*, "Carbon Nanotubes and its gas-sensing applications: A Review," *Sensors & Actuators A Physical*, vol. 291, pp. 107-143, Jun. 2019.
[31] Duoc Vo, Thanh Hung, Chu Manh *et al.*, "Room temperature highly toxic NO2 gas sensors based on rootstock/scion nanowires of SnO2/ZnO, ZnO/SnO2, SnO2/SnO2 and, ZnO/ZnO," *Sensors and Actuators B: Chemical*, vol. 348, pp. 130652, Sep. 2021
[32] Ao Liu, Siyuan Lv, Li Jiang, *et al.*, "The gas sensor utilizing polyaniline/ MoS2 nanosheets/ SnO2 nanotubes for the room temperature detection of ammonia," *Sensors and Actuators B: Chemical*, vol. 332, pp. 129444, Apr. 2021.

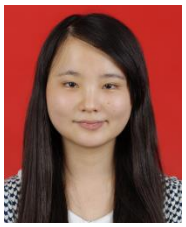

Anyan Jiang received her bachelor's degree in engineering in 2016 from Donghua University. Now she is currently pursuing her Doctor's degree in Chongqing University, Chongqing, China. Her main research interests include signal and information processing and gas sensing techniques.

Fengchun Tian received his B.Sc., M.Sc., and Ph.D. degrees in radio engineering, biomedical instruments and engineering, theoretical electric engineering from Chongqing University, Chongqing, P.R. China, in 1984, 1986, and 1996, respectively. Since 1984, he has been working in Chongqing University as a teacher. Since 2001, he has been a professor at Chongqing University. Since 2007, he has also been an adjunct professor in the University of Guelph, Canada. Currently, he is the director of Chongqing Key Laboratory of Bio-perception & Intelligent Information Processing. His research interests are artificial olfaction (electronic nose), image processing biomedical and modern signal processing technology.

James Anthony Covington (M'16) received the B.Eng. (Hons.) degree in electronic engineering and the Ph.D. degree from Warwick University in 1996 and 2000, respectively. His Ph.D. dissertation was on the development of CMOS and silicon-on-insulator CMOS gas sensors. He was a Research Fellow with Warwick University and Cambridge University on the development of gas and chemical sensors. He became a Lecturer at the School of Engineering, The University of Warwick, in 2002, and promoted to an Associate Professor in 2006, where he is currently a Professor of Electronic Engineering and the Head of the BioMedical Sensors Laboratory, School of Engineering. He has authored or co-authored over 170 journal articles and patents. His current research interests focus on the development of microanalysis systems, electronic noses, and ratification olfaction, employing a range of novel sensing materials, device structures, and microfabrication methods for applications with the environmental and medical application domains. More recently, based on his experience in gas sensing, he applied these skills in developing olfactory displays and related aroma-based technologies.

Maogang Jiang received a bachelor's degree in communication engineering in 2016, Shanghai Maritime University, Shanghai, China. Now he is currently pursuing for a master's degree at Chongqing University of Technology, Chongqing, China. His research interests are circuit and information processing.

Zhiyuan Wu received his master’s degree in biochemistry and molecular biology in 2020 from Fuzhou University. Now he is currently pursuing his Doctor’s degree in Chongqing University, Chongqing, China. His main research interests include electronic nose, gas sensing techniques and signal information processing.